

METALLICITY AND KINEMATIC DISTRIBUTIONS OF RED HORIZONTAL-BRANCH STARS FROM THE SDSS SURVEY

Y.Q. CHEN¹, G. ZHAO¹, J.K. ZHAO¹, X.X. XUE¹, W.J. SCHUSTER²

Draft version November 10, 2018

ABSTRACT

On the basis of a recently derived color-metallicity relation and stellar parameters from the Sloan Digital Sky Survey Data Release 7 spectroscopic survey, a large sample of red horizontal branch candidates have been selected to serve as standard candles. The metallicity and kinematic distributions of these stars indicate that they mainly originate from the thick-disk and the halo populations. The typical thick disk is characterized by the first group peaking at $[\text{Fe}/\text{H}] \sim -0.6$, $V_{\text{rot}} \sim 170 \text{ km s}^{-1}$ with a vertical scale height around $|Z| \sim 1.2 \text{ kpc}$, while stars with $[\text{Fe}/\text{H}] < -0.9$ are dominated by the halo population. Two sub-populations of the halo are suggested by the RHB stars peaking at $[\text{Fe}/\text{H}] \sim -1.3$: one component with $V_{\text{rot}} > 0 \text{ km s}^{-1}$ (Halo I) shows a sign of metallicity gradient in the $[\text{Fe}/\text{H}]$ versus $|Z|$ diagram, while the other with $V_{\text{rot}} < 0 \text{ km s}^{-1}$ (Halo II) does not. The Halo I mainly clumps at the inner halo with $R < 10 \text{ kpc}$ and the Halo II comes both from the inner halo with $R < 10 \text{ kpc}$ and the outer halo with $R > 10 \text{ kpc}$ based on the star distribution in the R versus $|Z|$ diagram.

Subject headings: stars:horizontal-branch – Galaxy: kinematics – Galaxy: the thick disk – Galaxy: the halo

1. INTRODUCTION

Red horizontal-branch (RHB) stars are found in many Galactic globular clusters (GCs) with intermediate metallicity $-1.7 < [\text{Fe}/\text{H}] < -0.3$ (see, e.g., Piotto et al. 2002). This metallicity range includes stars from the halo, the thick disk, the thin disk, and probably the bulge. Due to their nearly constant absolute magnitude, this type of stars constitutes an ideal sample to trace various Galactic populations in the Galaxy.

Generally, the identification of RHB stars in the field is rather difficult just by their colors but some attempts to identify this type of star had been made (Rose 1985; Tautvaisiene 1996; Preston 2006). However, these works did not produce a large sample of RHB stars (for example, a sample with star number larger than 100) for statistic work. With the aid of Hipparcos parallaxes, Kaempf et al. (2005) selected a large sample of RHB stars in the field and calculated their kinematical parameters based on available radial velocities and proper motions. They found two populations: a disk one having $|Z| \sim 0.6 \text{ kpc}$ and a halo one showing $|Z| \sim 4 \text{ kpc}$. This is the only work to trace the structure of the Galaxy via a large sample of RHB stars. Due to the distance limitation of the Hipparcos survey, these results were based on stars in the solar neighborhood, where the majority of the disk stars are from the thin disk with a minority from the thick disk and only a sprinkling of halo stars. It is of high interest to trace the disk and halo populations via RHB stars locating far away from the solar neighborhood and well above the Galactic plane. For this purpose, planned or ongoing kinematically unbiased surveys,

such as the Global Astrometric Interferometer for Astrophysics (GAIA; Turon et al. 2005), the SDSS/SEGUE (York et al. 2000; Yanny et al. 2009), and the LAMOST (Zhao et al. 2006) projects, will provide a chance to obtain and to study a large sample of RHB stars to the distant halo.

In this work, we attempt to investigate the properties of RHB stars and to carry out kinematic traces of various Galactic populations using RHB stars selected from the SDSS spectroscopic survey. As compared with the previous study by Kaempf et al. (2005), the present work has several advantages. First of all, the SDSS survey covers quite distant regions of the Galaxy, and our study can be extended far away from the solar neighborhood. Second, spectroscopic data of the SDSS survey provide stellar parameters, radial velocities, and metallicities. This data set not only makes it possible to identify RHB candidates more easily, but also provides the most powerful tool to investigate the Galactic populations by a combination of chemical and kinematical ingredients, in view of the fact that our Galaxy evolves both chemically and dynamically. Finally, it is expected that RHB stars selected from the SDSS survey could extend to a much lower metallicity range than that of Kaempf et al. (2005), which mainly concentrated on solar metallicity, and thus they will contribute much to the understanding of the thick-disk and the halo populations.

2. SELECTION OF RHB STARS

RHB stars are easily seen based on the color-magnitude diagrams (CMDs) of GCs, and statistically it is possible to pick out this type of star in the field of the solar neighborhood with the aid of Hipparcos parallaxes. Without previously-known distance information for stars far from the solar neighborhood, the selection of RHB stars in the field is rather difficult. But the problem of identification is much easier if the metallicity of the star is known, as shown in Straižys et al. (1981). Based on high resolution

¹ Key Laboratory of Optical Astronomy, National Astronomical Observatories, Chinese Academy of Sciences, Beijing, 100012, China; cyq@bao.ac.cn.

² Observatorio Astronómico Nacional, Universidad Nacional Autónoma de México, Apartado Postal 877, C.P.22800 Ensenada, B.C., México;schuster@astrosen.unam.mx

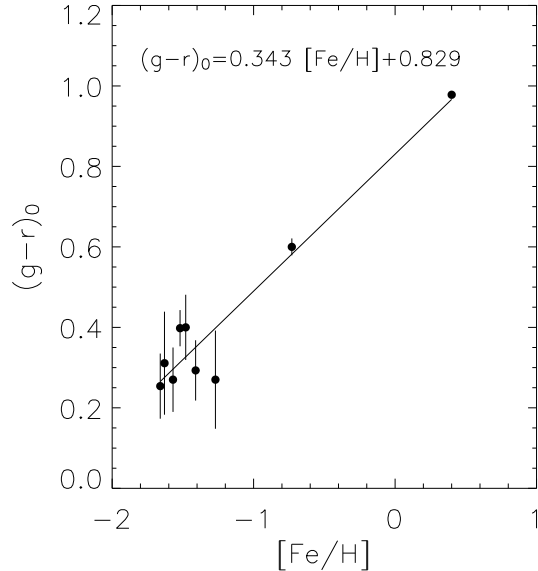


Figure 1. $(g-r)_0$ - $[\text{Fe}/\text{H}]$ diagram for clusters in Chen et al. (2009). The solid line indicates a linear fitting to the data.

and high signal-to-noise ratio spectra, around 30 RHB stars have been identified in the literature (e.g., Behr et al. 2003; Carney et al. 2003, 2008). In order to enlarge this sample, RHB stars have been identified from the SDSS low resolution ($R \sim 1800$) spectroscopic survey. The SDSS Data Release 7 (DR7; Abazajian et al. 2009) provides photometry and spectroscopic metallicities for a large sample of high-latitude stars, allowing the identification of a large sample of RHB stars in the field.

2.1. The Metallicity-Color Relation

As noticed in Chen et al. (2009), the $(g-r)_0$ values of RHB stars in metal-poor GCs with $[\text{Fe}/\text{H}] = -1.6$ dex, such as Pal 3, NGC 7006, and M3, are about 0.25-0.30 mag and extend to the red, reaching 0.60 in M71 with $[\text{Fe}/\text{H}] = -0.8$ and to 0.98 in NGC 6791 with $[\text{Fe}/\text{H}] = +0.4$. In fact, there is a correlation between $(g-r)_0$ and $[\text{Fe}/\text{H}]$ for RHB stars in clusters. In order to obtain a quantitative relation, we perform a linear regression to the data in Chen et al. (2009), which gives $(g-r)_0 = 0.343(\pm 0.039)[\text{Fe}/\text{H}] + 0.829$. The scatter around this relation is approximately 0.07 mag. Figure 1 shows the peaking $(g-r)_0$ (and its error) versus $[\text{Fe}/\text{H}]$ for each cluster and a linear relation is obtained by fitting to these points.

Assuming that RHB stars in the field follow the same $(g-r)_0$ and $[\text{Fe}/\text{H}]$ relation as these clusters, the first step is to apply this color-metallicity relation to all stars in SDSS-DR7 where spectroscopic metallicities and photometric colors are available in the published catalog. In the present work, the interstellar reddening values $E(B-V)$ are based on the extinction map of Schlegel et al. (1998) and we adopt the reddening corrections for $ugriz$ colors from Fukugita et al. (1996). In the selection, a deviation in $(g-r)_0$ to the above relation $\delta \leq 0.15$ mag is used to select stars; this value is adopted by taking into account an error of 0.2 dex in $[\text{Fe}/\text{H}]$ in SDSS-DR7, an error of 0.1-0.2 mag in the reddening uncertainty, and

an approximate $(g-r)_0$ color extension of 0.1 mag for RHB stars in cluster. Then, we select stars with signal-to-noise ratios of their spectra larger than 10 and metallicity larger than $[\text{Fe}/\text{H}] > -2.0$ so that their radial velocities and stellar parameters can be reliably determined from the SDSS-DR7 catalog. Finally, an upper cutoff at $g = 20$ mag is necessary because the proper motions from the USNO survey become seriously contaminated by misidentifications toward faint magnitudes according to Fuchs et al. (2009). But the effective cutoff in magnitude of our final sample is around $g = 18 - 18.5$ mag and the saturation flag in the SDSS-DR7 catalog is used to avoid stars whose magnitudes suffer from saturation effects. With these criteria, we obtain our preliminary sample of $\sim 120,000$ stars.

2.2. The T_{eff} versus $\log g$ diagram

Using the above $(g-r)_0$ - $[\text{Fe}/\text{H}]$ relation, blue horizontal branch (BHB) and RR Lyrae stars are excluded at the bluer colors, and red giant branch stars at the red limit, for a given metallicity. However, the sample is significantly contaminated by main-sequence stars (MS), turnoff (TO), and subgiant (SG) stars with the same metallicity; these can be distinguished if their luminosity or gravities are known. In the CMD of the clusters in Chen et al. (2009), at a given metallicity, RHB stars have brighter absolute magnitudes than those of MS/TO/SGB stars despite their similar colors, and the separation between RHB and MS/TO/SGB stars in absolute magnitude at a given color becomes larger as the metallicity decreases. In view of this, stellar parameters, i.e., temperature, gravity and metallicity, taken from the SDSS-DR7 catalog, can be used to identify RHB stars. The T_{eff} - $\log g$ diagram for the first 20000 stars in the preliminary sample and the corresponding contour map is shown in Figure 2. This figure shows that MS/TO/SG and RHB stars can be distinguished with RHB stars clumping over the range of 4500-5900 K in temperature and 1.8-3.5 dex in $\log g$, which are the selection criteria for our sample stars. In order to check these temperature and gravity ranges for RHB stars, we have compiled stellar parameters of previously identified RHB stars in the field and in clusters based on high resolution spectral analyses in the literature. Most works (Behr et al. 2003; Carney et al. 2003, 2008) agree with the ranges of 4600-6200 K in temperature and of 2.0-3.3 dex in $\log g$ for RHB stars, which are consistent with the defined ranges of RHB stars in Figure 2.

3. STELLAR DISTANCES AND SPACE VELOCITIES

3.1. Distances, proper motions, and radial velocity

Stellar distances have been calculated using the absolute magnitude-metallicity relation of $M_g = 0.492[\text{Fe}/\text{H}] + 1.39$ derived by Chen et al. (2009). We have compared them with distances derived from the i magnitude and M_i - $[\text{Fe}/\text{H}]$ calibration derived in Chen et al. (2009), and they give similar distances. The radial velocities and proper motions are based on values provided by the SDSS-DR7 catalog. Note that the proper motions in the SDSS-DR7 catalog have been corrected for the systematic error noticed by Munn et al. (2008). Finally, only stars with high quality data in photometry ($\sigma_g < 0.1$,

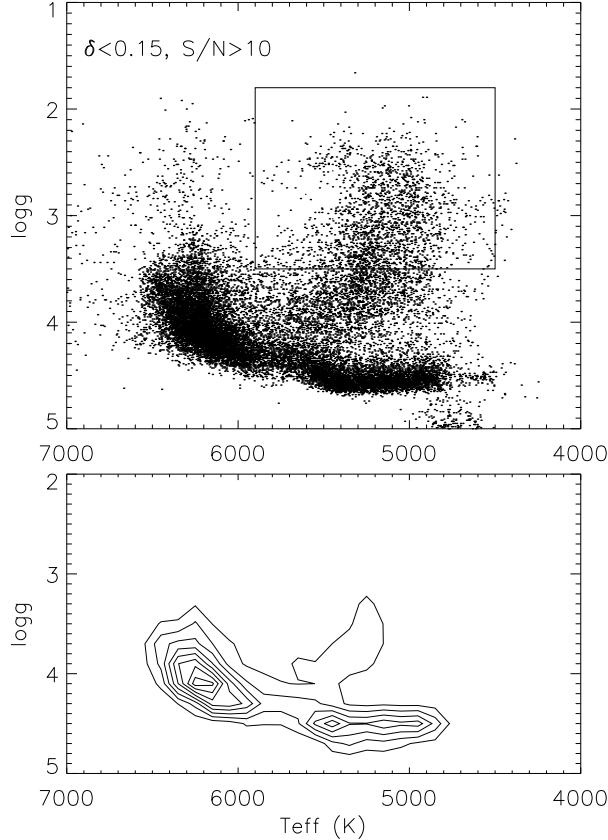


Figure 2. T_{eff} - $\log g$ diagram and its contour map for the first 20000 stars in the preliminary sample. The box indicates our selected RHB candidates.

$\sigma_i < 0.1$ mag), in proper motions ($\sigma_\mu < 3 \text{ mas yr}^{-1}$), and in radial velocity ($\sigma_{RV} < 10 \text{ km s}^{-1}$) are included in the sample.

3.2. Spatial velocity

Stellar positions (X,Y,Z) and heliocentric space velocity (U,V,W) are calculated following the same procedures as in Chen et al. (2000). We use a left-handed system in which U is positive toward the Galactic anti-center. The solar motion of (U,V,W)_⊙ = (7.5, 13.5, 6.8) km s^{-1} with respect to the LSR from Francis & Anderson (2009) and the local standard of rest (LSR) velocity of 220 km/s (corresponding to $V_{\text{hel}} \sim -225 \text{ km s}^{-1}$) are adopted in the present work.

The errors in spatial velocity come from the uncertainties of radial velocity, proper motion and distance. The error in radial velocity of 3 km/s corresponds to a spatial velocity error of 5 km s^{-1} . The distance error of 10%, estimated from an error in absolute magnitude of 0.2 mag , corresponds to a velocity error of 5-15 km s^{-1} . The largest error comes from uncertain proper motions. As shown in Ivezić et al. (2008), a random error of 3 mas yr^{-1} in proper motions will lead to a velocity error of about 15 km s^{-1} at a distance of 1 kpc and about 80 km s^{-1} at a distance of 5 kpc. Although the total error in spatial velocity is quite large, the data still represent usable measurements for a large sample because

the systematic errors are much smaller ($\sim 10 \text{ km s}^{-1}$ at a distance of 7 kpc) according to Ivezić et al. (2008).

In principle, a total velocity larger than 600 km s^{-1} is unreasonable, or indicates stars unbound to our Galaxy. Such stars are usually excluded from the final sample (e.g., Klement et al. 2009). In the present work, we keep them in our sample for further check, but we have checked that the main results are generally the same when we excluded them from the sample. With this in mind, we avoid to overexplain the results based on the spatial velocities only and instead statistical results based on metallicity and distance to the Galactic plane ($|Z|$) are more favorable in the following analysis.

The final sample includes 5391 stars for further analyses. Figure 3 shows the distributions of distances, g magnitude, reddening, and galactic latitudes of the final sample. Their identifications, stellar parameters, and spatial velocities are published electronically and a sample table consisting of the first 10 stars is presented in Table 1.

4. RESULTS AND DISCUSSIONS

4.1. The metallicity and kinematical distributions

By choosing a single stellar type, RHB stars, it is interesting to investigate the metallicity distribution and compare our results with those from other types of stars, e.g., MS or TO stars. In Figure 4, a histogram of our sample shows two peaks in the metallicity distribution with a division at $[\text{Fe}/\text{H}] \sim -0.9$ dex. Two Gaussian fits to the distribution show a metal-poor sub-population at $[\text{Fe}/\text{H}] \sim -1.3$ dex, and a metal-mild sub-population at $[\text{Fe}/\text{H}] \sim -0.6$ dex. As compared with the result from MS stars within 4 kpc of the Sun in the SDSS I and II survey by Carollo et al. (2010), we find that the two peaks in the metallicity distribution are quite similar. They suggested that stars in the metal-mild peak belong to the disk population (mainly the thick disk), while stars in the metal-poor peak belong to the halo population. However, there are some differences in star numbers for each population between RHB stars in the present work and MS stars in Carollo et al. (2010). In our work, the metal-poor component, peaking at $[\text{Fe}/\text{H}] \sim -1.3$, outnumbers the metal-mild component, peaking at $[\text{Fe}/\text{H}] \sim -0.6$, which is opposite to the result in Carollo et al. (2010), where the metal-mild component surpasses the metal-poor component. This is easily understood considering that their sample of stars is limited to $d < 4$ kpc from the Sun, and thus the disk population contributes significantly to their sample, while RHB stars in our sample have brighter absolute magnitudes and extend to more distant regions of the Galaxy where the halo dominates.

The variations in the metallicity distribution with different distances to the Galactic plane ($|Z|$) are shown in Figure 5, where the metallicity peak shifts from $[\text{Fe}/\text{H}] \sim -0.4$ dex for $|Z| < 1.5$, $[\text{Fe}/\text{H}] \sim -0.6$ dex for $1.5 \leq |Z| \leq 5$ to $[\text{Fe}/\text{H}] \sim -1.3$ dex for $|Z| > 8$. At $5 \leq |Z| \leq 8$, the star numbers between the two components are comparable. Note that the result in Figure 20 of Carollo et al. (2010) shows the shift of the metallicity peak from -0.6 at $0 \text{ kpc} < |Z| < 1 \text{ kpc}$, to -1.3 at $3 \text{ kpc} < |Z| < 4 \text{ kpc}$, reaching to -1.6 at $6 \text{ kpc} < |Z| < 7 \text{ kpc}$ and to -2.2 at $|Z| > 9 \text{ kpc}$. Therefore, the exact $[\text{Fe}/\text{H}]$ peaks at a given $|Z|$ between Carollo et al. (2010) and

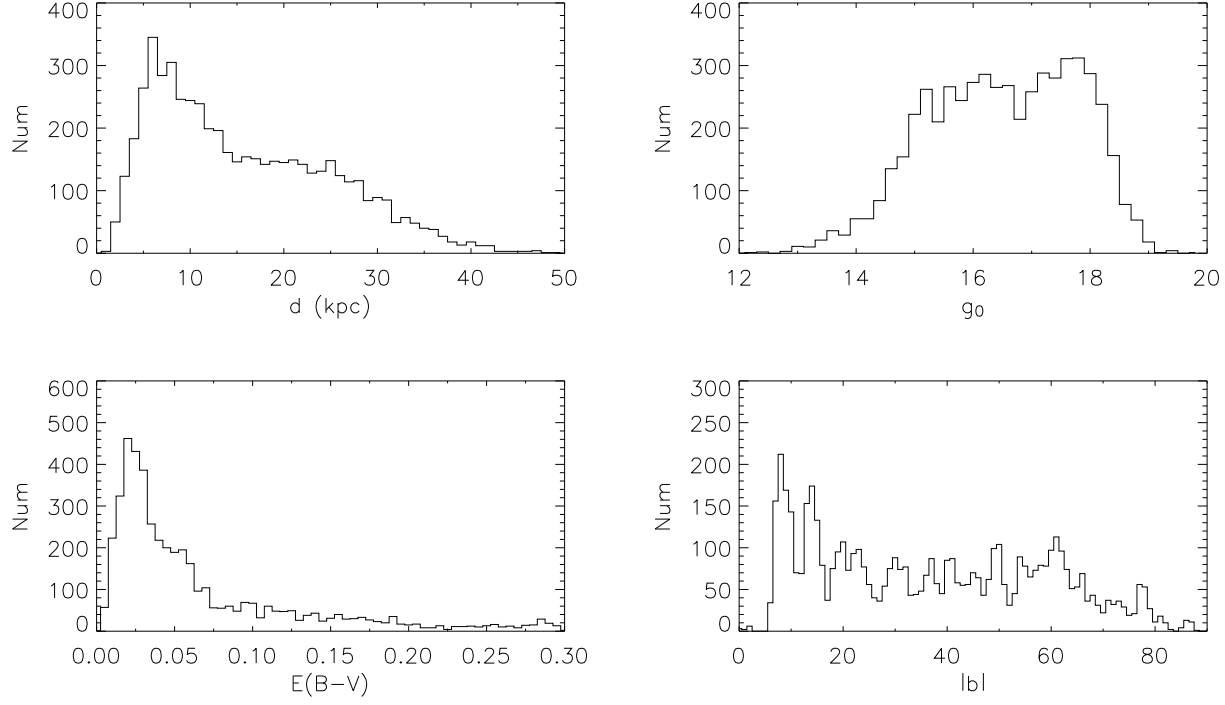


Figure 3. Distributions of distances, g_0 magnitude, reddening and galactic latitudes of the final sample.

Table 1

Identifications, stellar parameters, coordinates, and spatial velocities of the first ten stars in the final sample are presented.

plate	mjd	fiber	[Fe/H]	Z	d	g_0	RA	DEC	l	b	U	V	W
				(kpc)	(kpc)	(mag)	(deg)	(deg)	(deg)	(deg)	(km s^{-1})	(km s^{-1})	(km s^{-1})
408	51821	528	-0.40	-1.76	2.26	12.9	40.40	1.24	170.43	-51.18	-12.2	-36.0	14.7
573	52325	351	-0.48	3.44	4.99	14.6	150.36	4.35	234.60	43.54	192.4	-30.2	-53.8
580	52368	25	-0.47	4.70	5.70	14.9	166.10	4.22	250.11	55.70	147.6	-43.0	24.1
934	52672	473	-0.26	2.77	4.51	14.5	131.64	35.58	187.48	37.86	-27.7	-137.4	-99.4
1246	54478	542	-0.54	-0.94	3.90	14.1	86.88	0.52	205.03	-13.94	102.5	9.8	-22.4
1247	52677	590	-0.26	-0.61	2.78	13.5	88.28	0.60	205.62	-12.66	16.8	-42.5	23.8
1662	52970	136	-0.33	-0.61	4.05	14.3	351.21	51.95	109.63	-8.67	-132.2	-45.1	55.0
1910	53321	27	-1.25	-5.46	6.37	14.8	345.85	-9.63	62.27	-59.09	-63.8	-622.0	-351.3
1910	53321	276	-0.73	-4.64	5.50	14.7	343.82	-9.62	59.97	-57.50	304.3	-360.5	-199.8
1960	53289	416	-0.46	-1.51	3.31	13.7	322.40	12.24	65.01	-27.19	-84.4	-99.1	38.3

the present work are somewhat different due to the selection of different spectral types of stars in the sense that MS/TO stars in their sample include significant contributions from the thin disk and the halo with $[\text{Fe}/\text{H}] < -1.6$, while our sample of RHB stars has the largest contribution from the thick disk, the minority contribution from the halo and nearly negligible contribution from the thin disk.

In order to investigate the origins of the two populations in the metallicity distribution for RHB stars in the present work, the Toomre diagrams for stars with $[\text{Fe}/\text{H}] > -0.9$ and $[\text{Fe}/\text{H}] < -0.9$ are shown in Figure 6 where the solid circle indicates the division between the thick disk and the halo with $V_{\text{tot}} = 210 \text{ km s}^{-1}$ following Nissen & Schuster (2010). Note that there is a significant number of stars with a total velocity larger than 600 km s^{-1} in these figures due to the very large errors in

the determination of space velocities when the distance of the star is larger than 10 kpc. Therefore, we do not attempt to draw any firm conclusion from the kinematical data, but the statistical argument for dividing stars into different groups may be right.

It is clear that the metal-mild component of RHB stars clumps within the thick-disk region with some extension to the thin-disk region, while the majority of stars in the metal-poor component are located in the halo region. This result is consistent with that of Carollo et al. (2010) in the sense that the metal-mild component, peaking at $[\text{Fe}/\text{H}] \sim -0.6$, mainly originates from the thick disk and the metal-poor component, peaking at $[\text{Fe}/\text{H}] \sim -1.3$, generally belongs to the halo. In Figure 7, it is interesting to compare the kinematic diagrams between the two metallicity peaks for stars with $5 \text{ kpc} < |Z| < 8 \text{ kpc}$ in Figure 6 (the third panel). Again, it shows that

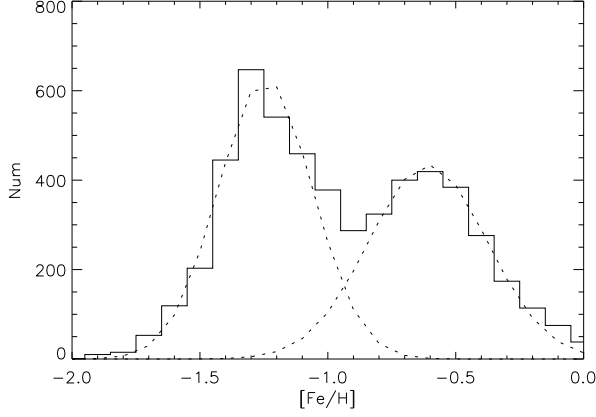


Figure 4. Metallicity distributions of RHB stars. The dotted lines show the Gaussian fits to the two populations separated by the metallicity division at $[\text{Fe}/\text{H}] \sim -0.9$.

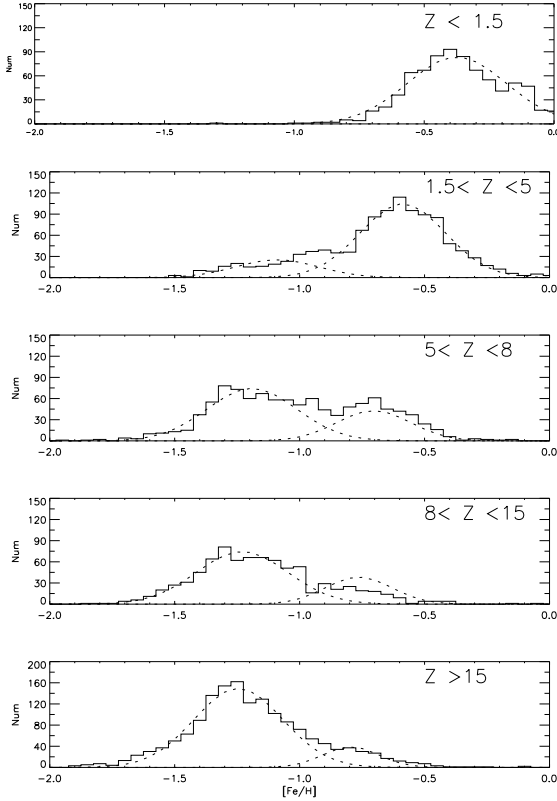


Figure 5. Metallicity distributions of RHB stars at different $|Z|$.

the metal-poor component at $[\text{Fe}/\text{H}] \sim -1.3$ mainly has the halo kinematics and the metal-mild component at $[\text{Fe}/\text{H}] \sim -0.6$ has the thick disk kinematics. In the following sections, we separate the stars into two parts with $[\text{Fe}/\text{H}] > -0.9$ and $[\text{Fe}/\text{H}] < -0.9$, respectively.

4.2. The $[\text{Fe}/\text{H}]$ versus $|Z|$ diagram

Figure 8 shows the distribution of 5391 RHB stars in the $[\text{Fe}/\text{H}]$ versus $|Z|$ diagram with the pink color corresponding to a high density, green to middle density, and black to the lowest density. The division be-

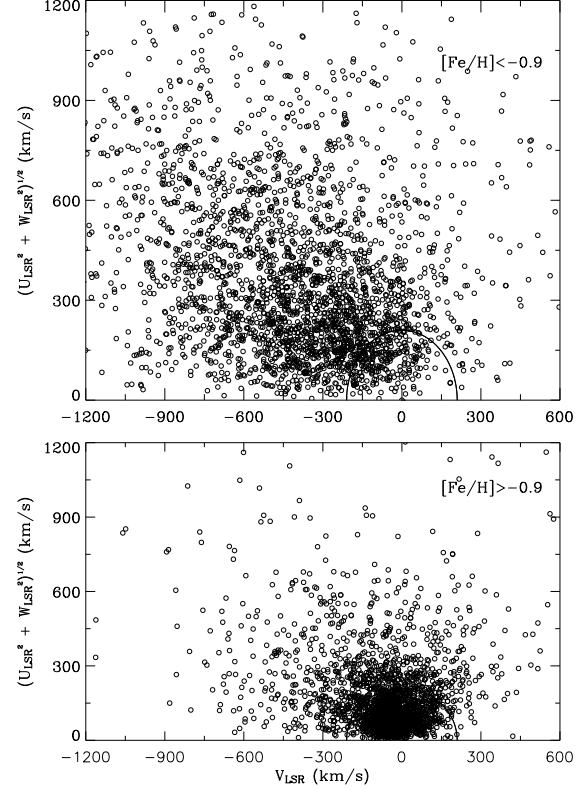


Figure 6. Toomre diagrams of RHB stars for $[\text{Fe}/\text{H}] > -0.9$ and $[\text{Fe}/\text{H}] < -0.9$. The circles indicate the division between the thick disk and the halo following Nissen & Schuster (2010).

tween the thick disk and the halo seems to be quite clear in the $[\text{Fe}/\text{H}]$ versus $|Z|$ diagram as clearly shown in Figure 8, where the edge of the thick disk could be as high as $|Z| \sim 8$ kpc at $[\text{Fe}/\text{H}] \sim -0.6$ and reduces to $|Z| \sim 2$ kpc at $[\text{Fe}/\text{H}] \sim -1.5$. Figure 9 (upper panel) shows individual stars in this diagram. It seems that there is a metallicity gradient in the vertical direction of the Galaxy, but the scatter around the gradient is quite large. The $|Z|$ range increases with decreasing metallicity probably due to the overlapping metallicity of stars from the halo, the thick-disk and the thin-disk populations at this metallicity range. Actually, the metallicity gradient is more significant in the middle metallicity range of $-1.2 < [\text{Fe}/\text{H}] < -0.4$ than the two outer ranges in this $[\text{Fe}/\text{H}]$ versus $|Z|$ diagram.

In order to investigate the properties of the thick-disk population, we try to exclude the contribution from the halo population and plot in the lower panel of Figure 9 the $[\text{Fe}/\text{H}]$ versus $|Z|$ diagram for stars with $|Z| < 5$ kpc and $[\text{Fe}/\text{H}] > -0.9$, which mainly originate from the thick disk. This figure shows that the trend in the $[\text{Fe}/\text{H}]$ versus $|Z|$ diagram is quite significant and the scatter around the gradient is greatly reduced. A linear regression to the data indicates a relation of $[\text{Fe}/\text{H}] = -0.292(\pm 0.012)|Z| + 0.116$ with a scatter of 0.037 dex. Taking into account the fact that a few points with $[\text{Fe}/\text{H}] > -0.35$ do not follow the above trend and may belong to the thin disk, they are excluded from the fitting, and the result is

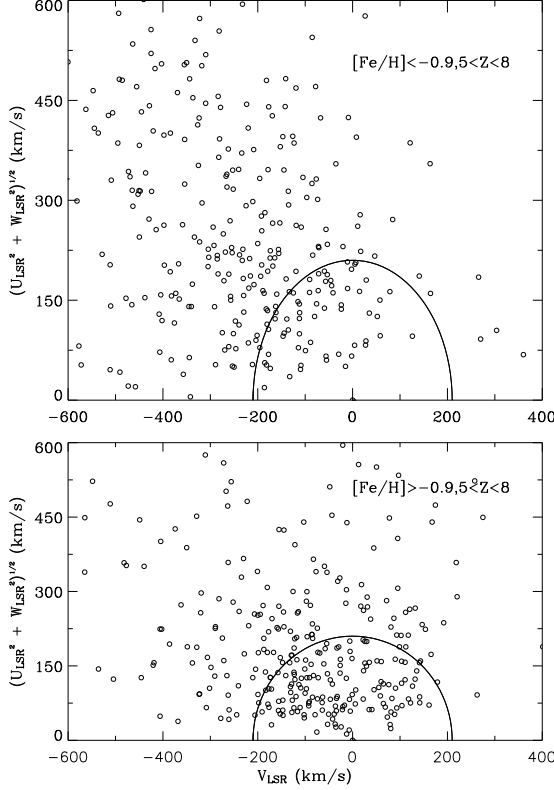


Figure 7. Toomre diagrams of RHB stars with $5 < |Z| < 8$ kpc for $[\text{Fe}/\text{H}] > -0.9$ and $[\text{Fe}/\text{H}] < -0.9$, respectively. The symbols are the same as Figure 6.

$[\text{Fe}/\text{H}] = -0.255(\pm 0.014)|Z| + 0.020$ with a scatter of 0.023 dex. The six points with $[\text{Fe}/\text{H}] > -0.35$ follow the trend of $[\text{Fe}/\text{H}] = -0.467(\pm 0.083)|Z| + 0.323$ with a scatter of 0.031 dex for $|Z| < 1.5$ kpc.

4.3. The V_{rot} versus $|Z|$ diagrams

Figure 10 shows the kinematical gradients, V_{rot} ($= V + 220 \text{ km s}^{-1}$) versus $|Z|$, and Figures 11 and 12 show the U and W velocities versus $|Z|$ for RHB stars; for both figures, $[\text{Fe}/\text{H}] < -0.9$ and $[\text{Fe}/\text{H}] > -0.9$ in the upper and lower panels, respectively. These figures show that $\langle U \rangle$ and $\langle W \rangle$ velocities generally do not vary much with $|Z|$, independent of metallicity, while for $[\text{Fe}/\text{H}] < -0.9$ the $\langle V_{\text{rot}} \rangle$ tends to decrease with increasing $|Z|$ for the region $|Z| < 10$ kpc and becomes flat for the region $|Z| > 10$ kpc. The rotational-velocity gradients are approximately $-30 \text{ km s}^{-1} \text{ kpc}^{-1}$ for stars with $[\text{Fe}/\text{H}] < -0.9$ and $|Z| < 10$ kpc, and about $-19 \text{ km s}^{-1} \text{ kpc}^{-1}$ for stars with $[\text{Fe}/\text{H}] > -0.9$ and $|Z| < 15$ kpc.

Quantitatively, different authors give somewhat different gradients for $|Z| < 5$ kpc. For example, Carollo et al. (2010, in their Figure 11) found a decreasing $\langle V_{\phi} \rangle$ with $|Z|$ for stars with $-0.8 < [\text{Fe}/\text{H}] < -0.6$ and $|Z| < 4$ kpc with a rotational-lag gradient of $-36 \text{ km s}^{-1} \text{ kpc}^{-1}$. Chiba & Beers (2000) found a rotational-lag gradient of $-30 \text{ km s}^{-1} \text{ kpc}^{-1}$ based on a large sample of stars (~ 1200) with $|Z| \lesssim 2$ kpc. Allende Prieto et al. (2006) adopted SDSS photometric distances and radial velocities (without using proper motions), and found a

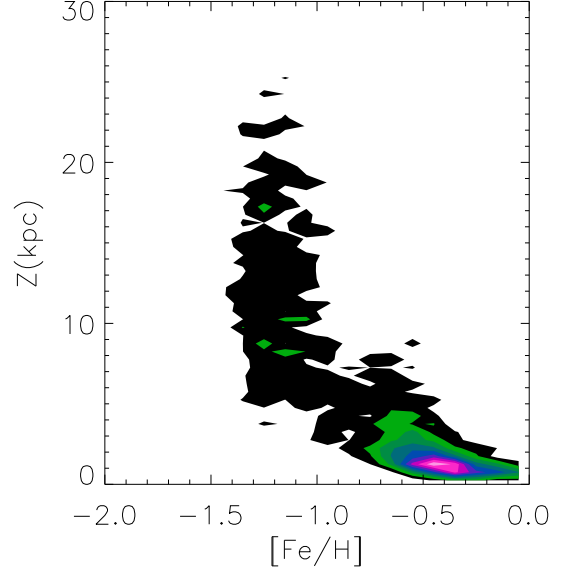


Figure 8. Distribution of 5391 RHB stars in the $[\text{Fe}/\text{H}]$ vs. $|Z|$ diagram. The star density decreases as the color varies from the pink, the blue, the green to the black.

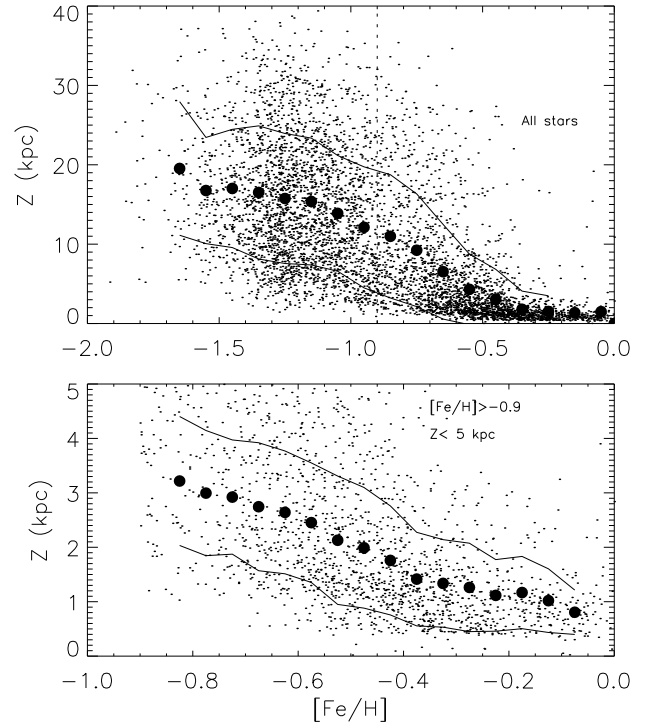


Figure 9. $[\text{Fe}/\text{H}]$ vs. $|Z|$ diagram for the full sample (upper panel) and for stars with $[\text{Fe}/\text{H}] > -0.9$ and $|Z| < 5$ kpc (lower panel). The mean $|Z|$ at a given $[\text{Fe}/\text{H}]$ and the scatter are shown by the large filled circles and solid lines, respectively.

rotational-lag gradient of $-16 \text{ km s}^{-1} \text{ kpc}^{-1}$ for stars between $|Z| = 1$ and 3 kpc. In Majewski (1992), the value is $-21 \text{ km s}^{-1} \text{ kpc}^{-1}$ based on deep proper-motion survey of the Galaxy out to $|Z| \sim 6$ kpc. Our value of $-19 \text{ km s}^{-1} \text{ kpc}^{-1}$ for stars with $[\text{Fe}/\text{H}] > -0.9$ and $|Z| < 15$

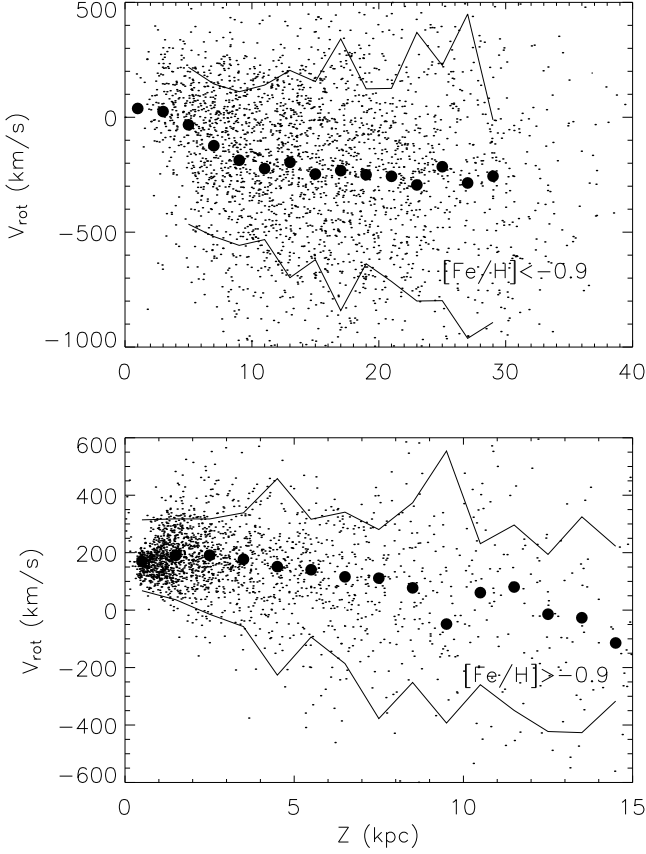


Figure 10. V_{rot} versus $|Z|$ for stars with $[\text{Fe}/\text{H}] < -0.9$ and $[\text{Fe}/\text{H}] > -0.9$ (upper and lower panels, respectively).

kpc is quite consistent with previous values within the error range.

It has been suggested that the rotational lag and the velocity dispersions vary with distance from the Galactic plane (Majewski 1994). However, our work shows that, for $[\text{Fe}/\text{H}] < -0.9$, the $\langle V_{\text{rot}} \rangle$ decreases with increasing $|Z|$ for the region of $|Z| < 10$ kpc, while for $|Z| > 10$ kpc, where the halo dominates, there is no significant trend. In Bond et al. (2010) the halo population with $[\text{Fe}/\text{H}] < -1.1$ does not show any trend in the $\langle V_{\text{rot}} \rangle$ with $|Z|$ over the region of $|Z| < 5$ kpc, which does not agree with our result for $[\text{Fe}/\text{H}] < -0.9$ and $|Z| < 10$ kpc. This discrepancy may be easily understood if we assume that stars with $[\text{Fe}/\text{H}] < -0.9$ in the present work consist of two halo sub-populations. Finally, the scatters around these trends in Figure. 10-12 are rather large, and further studies with larger samples and high-quality data are needed.

4.4. The $[\text{Fe}/\text{H}]$ vs. V_{rot} diagram

As described above, this diagram is a useful way to trace the structure of the Galaxy when abundance and kinematical data are combined. Figure 13 shows the histograms of V_{rot} (upper panel) and the $[\text{Fe}/\text{H}]$ versus V_{rot} diagram (lower panel) for RHB stars. The upper panel shows that the metal-mild component peaks at $V_{\text{rot}} \sim 170 \text{ km s}^{-1}$ and the metal-poor component spans a wide range in V_{rot} without any sharp peak. That is,

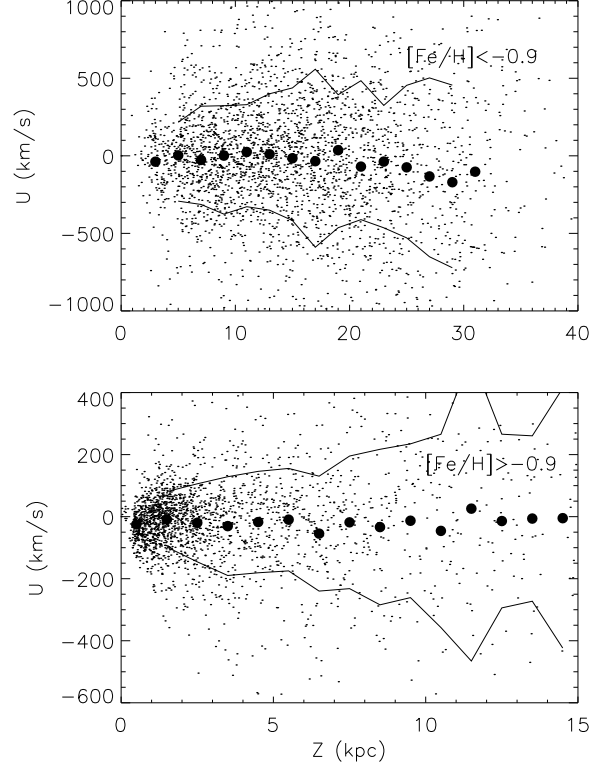


Figure 11. U velocities vs. $|Z|$ for stars with $[\text{Fe}/\text{H}] < -0.9$ and $[\text{Fe}/\text{H}] > -0.9$ (upper and lower panels, respectively).

the V_{rot} dispersion in the former is smaller than the latter component. This is expected in the context of the Galactic stellar populations with the halo population with $[\text{Fe}/\text{H}] < -1.0$ having a large velocity dispersion as compared to the thick-disk population, with a metallicity peak at $[\text{Fe}/\text{H}] \sim -0.6$, and the thin-disk population with a metallicity peak at $[\text{Fe}/\text{H}] \sim -0.2$. Actually, the distribution in V_{rot} for the metal-poor component is rather broad and in this work we separate the metal-poor component into two groups with $V_{\text{rot}} > 0 \text{ km s}^{-1}$ and $V_{\text{rot}} < 0 \text{ km s}^{-1}$ in the lower panel of Figure 13. The metal-mild population with $[\text{Fe}/\text{H}] \sim -0.6$ has a peak at $V_{\text{rot}} \sim 170 \text{ km s}^{-1}$, which is quite similar to that derived from the solar neighborhood by Soubiran et al. (2003), who derive a rotational lag (Stromberg asymmetrical drift) of $V_{\text{lag}} \sim 51 \text{ km s}^{-1}$ with respect to the LSR, and is somewhat lower than the average rotational lag of $V_{\text{lag}} \sim 80 \text{ km s}^{-1}$ by Fuhrmann (1998) for a group of 16 thick-disk stars. For the metal-poor population, we separate them into two sub-populations with the division of stars with $V_{\text{rot}} > 0 \text{ km s}^{-1}$ being “Halo I” and stars with $V_{\text{rot}} < 0 \text{ km s}^{-1}$ being “Halo II”. In Figure 14, the $[\text{Fe}/\text{H}]$ versus $|Z|$ diagrams for the Halo I and II sub-populations are shown in the upper and lower panels, respectively. It shows that there is a hint of metallicity gradient in the Halo I, as for the thick-disk population, while for the Halo II population the metallicity gradient is much weaker, if it exists at all. This gives concordance to our separation of the halo population into the Halo I and the Halo II components for stars with $[\text{Fe}/\text{H}] < -0.9$ in Figure 13.

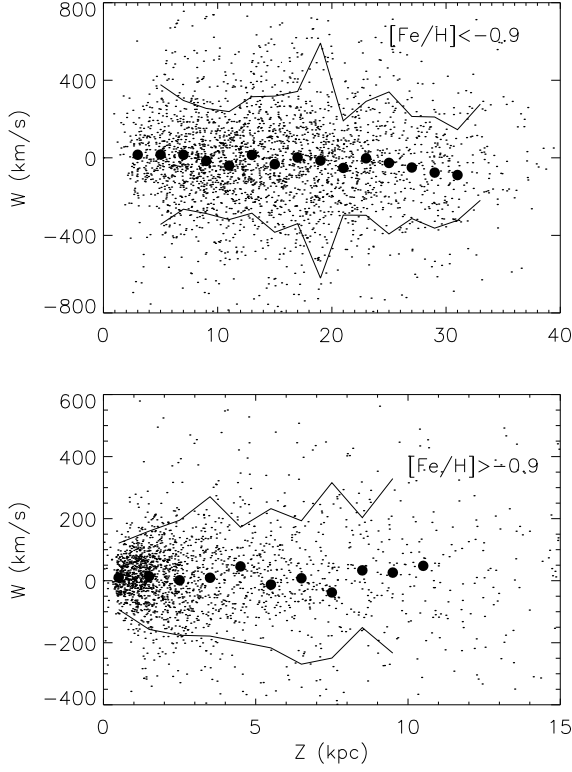


Figure 12. W velocities vs. $|Z|$ for stars with $[\text{Fe}/\text{H}] < -0.9$ and $[\text{Fe}/\text{H}] > -0.9$ (upper and lower panels, respectively).

Actually, the division of the halo at $V_{\text{rot}} \sim 0 \text{ km s}^{-1}$ is consistent with the result of Carollo et al. (2007), who found an inner halo with a slightly prograde rotation and a outer halo with a net retrograde. In their Figure 5, the division between the inner and the outer halo is quite clear in the $R - |Z|$ diagram. In view of this, it is interesting to investigate the division for the halo population based on RHB stars. Figure 15 shows the distribution of RHB stars for the Halo I and the Halo II sub-populations in the $R - |Z|$ diagram. The main result from this figure is that the Halo I stars clump within $R < 10 \text{ kpc}$ and $|Z| < 10 \text{ kpc}$, while the Halo II stars show two clumps with one within 10 kpc and the other grouping outside 10 kpc. In this sense, we favor the suggestion that the transition between the inner halo and the outer halo is around 10 kpc. Note that the Figure 5 of Carollo et al. (2007) is divided by the metallicity while our Figure 15 is separated by the rotation, and thus the comparison between the two works is not direct. However, the structure of the halo consisting the inner and the outer parts is the same.

4.5. Implications for the evolution of the Galaxy

Since the first suggestion for the thick disk in our Galaxy was made on the basis of star counts by Gilmore & Reid (1983), a considerable number of studies have helped to characterize the Galaxy's thick-disk component, in an effort to deduce its origin and better understand its nature. Most works suggest that the thick disk consists of old ($\gtrsim 10 \text{ Gyr}$) stars of intermediate metallicities, ($-1.0 \lesssim [\text{Fe}/\text{H}] \lesssim -0.2$) with a rotational lag of ≈ 50

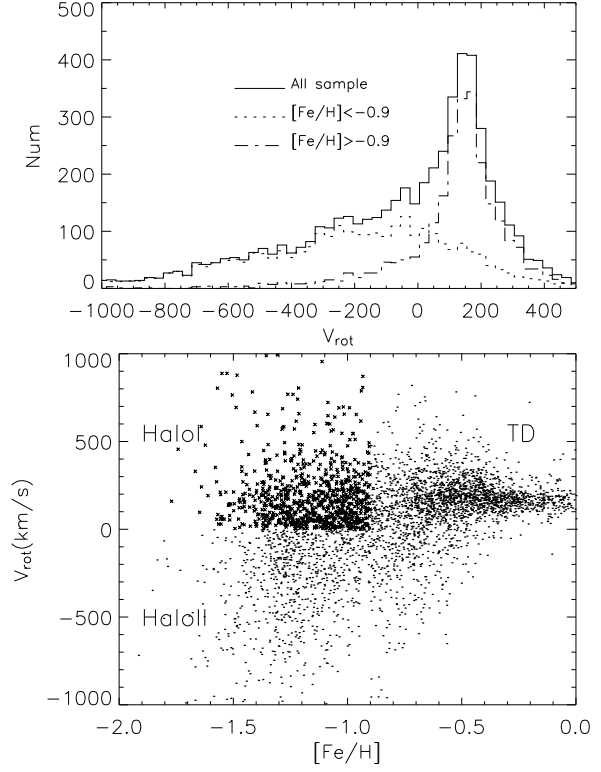


Figure 13. Histograms of V_{LSR} (upper panel) and the $[\text{Fe}/\text{H}]$ versus V_{LSR} diagram (lower panel). The thick-disk population consists of stars with $[\text{Fe}/\text{H}] > -0.9$, while the halo population is divided into two sub-populations, the Halo I (crosses) and the Halo II (dots).

km s^{-1} , and a scale height between 0.8 and 1.2 kpc. Our results from RHB stars with $[\text{Fe}/\text{H}] < -0.9$ dex are generally consistent with these numbers; this population peaks at $[\text{Fe}/\text{H}] \sim -0.6 \pm 0.2$ dex, $V_{\text{rot}} \sim 170 \pm 20 \text{ km s}^{-1}$, and a vertical scale height of $1.2 \pm 0.3 \text{ kpc}$.

However, the thick disk may have a metal-weak component (MWTD) (e.g., Beers et al. 2002). Based on MS/TO stars from the SDSS survey, Ivezić et al. (2008) reveal a feature consisting of stars of $[\text{Fe}/\text{H}] \sim -1.0$ dex and $|Z| \sim 2 - 3 \text{ kpc}$, which they classified as the MWTD population. Brown et al. (2008) presented a complete spectroscopic survey of 2414 Two Micron All Sky Survey (2MASS)-selected BHB candidates selected over 4300 deg^2 of the sky and found that the BHB stars located at a distance from the Galactic plane $|Z| < 4 \text{ kpc}$ trace what is clearly a metal-weak thick-disk population, with a mean metallicity of $[\text{Fe}/\text{H}] = -1.7$ dex. But the existence of MWTD among BHB stars with $|Z| < 4 \text{ kpc}$ is not confirmed by their further work in the paper by Kinman et al. (2009).

In the present work, the MWTD has not been found as shown in Figure 14 (upper panel), where there are only a few stars with $[\text{Fe}/\text{H}] < -0.9$ and $|Z| < 5 \text{ kpc}$, and very few with $|Z| < 2 \text{ kpc}$. The Halo I sub-population with $[\text{Fe}/\text{H}] \sim -1.3$ and $V_{\text{rot}} > 0 \text{ km s}^{-1}$, generally has $|Z| > 5 \text{ kpc}$. Since it is well accepted that the edge of the thick disk is at about 5.5 kpc above the Galactic plane as suggested by Majewski (1994), and since we have measured a scale height for the thick disk of $|Z| =$

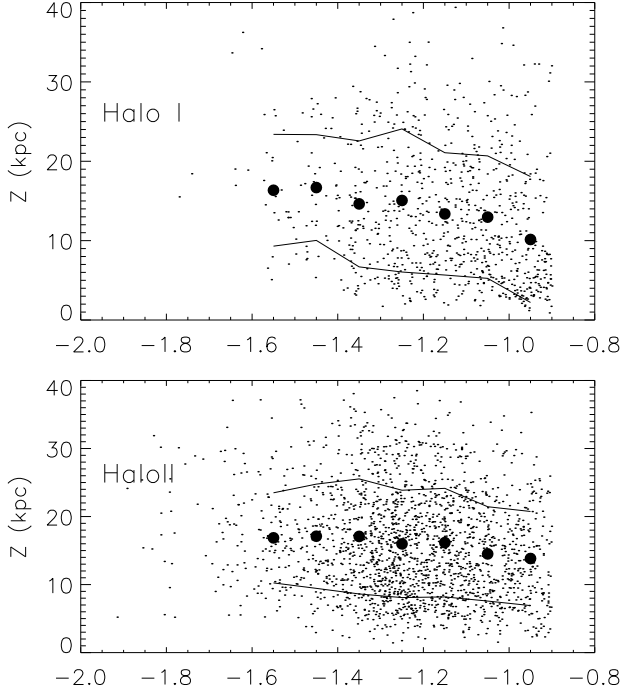


Figure 14. $[\text{Fe}/\text{H}]$ vs. $|Z|$ for the Halo I (upper panel) and II (lower panel) sub-populations.

1.2 ± 0.3 kpc, we suggest this sub-population, Halo I, really corresponds to the halo.

In connection with the halo population, our result confirms with the existence of the inner and the outer halo sub-population in the $R - |Z|$ diagram. From the $[\text{Fe}/\text{H}] - |Z|$ diagram, it hints that the inner halo shows a metallicity gradient while the outer halo does not. From our data, we cannot detect any sign of stellar streams reported before due to the selection effect of the spectroscopic survey of the SDSS project and the star number in our sample is too small for detecting any overdensity produced by stellar streams.

5. CONCLUSIONS

Based on photometric and spectral data, a group of RHB stars have been selected from the SDSS survey, whose distances can be estimated by using the calibrations from Chen et al. (2009). Combining with available proper motions from the USNO survey and radial velocities from the SDSS survey, the space velocities (U, V, W) have been calculated for a sample of 5391 RHB stars, and their metallicities and kinematical gradients have been investigated in order to trace the evolution of the Galaxy. The main results are as follows. (1) There are two peaks in the metallicity distributions of RHB stars with a division at $[\text{Fe}/\text{H}] \sim -0.9$. Stars with $[\text{Fe}/\text{H}] > -0.9$, centered at $[\text{Fe}/\text{H}] \sim -0.6$, correspond to the thick-disk population, while stars with $[\text{Fe}/\text{H}] < -0.9$, peaking at $[\text{Fe}/\text{H}] \sim -1.3$, have generally halo kinematics in the Toomre diagram. The metallicity gradient for thick disk stars with $-0.9 < [\text{Fe}/\text{H}] < -0.3$ is significant with $[\text{Fe}/\text{H}] = -0.255|Z| + 0.02$. RHB stars from the thick disk with $|Z| < 5$ kpc have a peak metallicity of $[\text{Fe}/\text{H}] \sim -0.6$ dex, a peak rotation velocity of

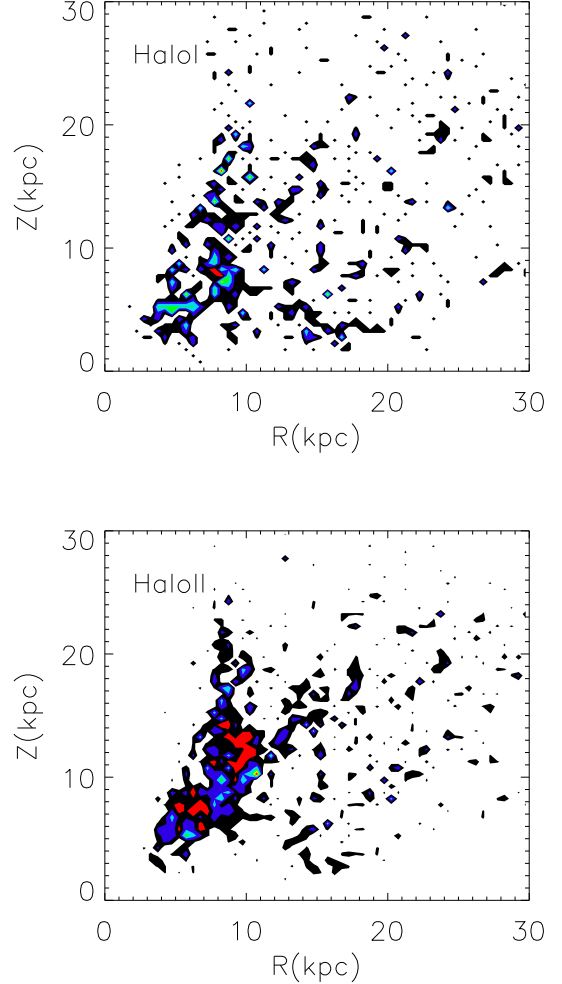


Figure 15. R vs. $|Z|$ diagrams for the Halo I (upper panel) and Halo II (lower panel) sub-populations.

$V_{\text{rot}} \sim 170 \text{ km s}^{-1}$, and a vertical scale height of $|Z| \sim 1.2$ kpc. (2) The division between the thick disk and the halo seems to be quite clear in the $[\text{Fe}/\text{H}]$ versus $|Z|$ diagram as clearly shown in Figure 8, where the edge of the thick disk could be as high as $|Z| \sim 8$ kpc at $[\text{Fe}/\text{H}] \sim -0.6$ and reduces to $|Z| \sim 2$ kpc at $[\text{Fe}/\text{H}] \sim -1.5$. Meanwhile, there is a detectable rotational gradient in the thick disk and a nearly constant Galactic rotation in the halo in the vertical direction to the Galactic plane. (3) Two halo sub-populations have been identified, the Halo I and the Halo II, for stars peaking at $[\text{Fe}/\text{H}] \sim -1.3$, based on the V_{rot} and the $[\text{Fe}/\text{H}] - |Z|$ diagram. The Halo I mainly clumping at $R < 10$ kpc with a sign of metallicity gradient, while the Halo II clumping at two regions, both $R < 10$ kpc and $R > 10$ kpc, shows a negligible metallicity gradient.

The above results are somewhat limited by the presence of substantial scatter around these relations, which probably derives mainly from the large errors of the proper motions, and the limited sample of RHB stars with precise and accurate proper motions. Further study on a large sample of RHB stars with accurate proper motions is desirable to clarify the two halo sub-populations.

In particular, the distance and proper-motion data for distant stars may be provided by the GAIA project. Combining these with the upcoming LAMOST spectroscopic survey, we hope to identify more RHB stars and to analyze the RHB sample for structure in the metallicities, spatial coordinates, and Galactic velocities.

This work has been supported by the National Natural Science Foundation of China under grants 10673015 and 10821061, the National Basic Research Program of China (973 program) 2007CB815103/815403, the Academy program 2006AA01A120, the Youth Foundation of National Astronomical Observatories of China, and the CONA-CyT project CB-2005/49434 (Mexico).

Funding for the Sloan Digital Sky Survey (SDSS) and SDSS-II has been provided by the Alfred P. Sloan Foundation, the Participating Institutions, the National Science Foundation, the US Department of Energy, the National Aeronautics and Space Administration, the Japanese Monbukagakusho, the Max Planck Society, and the Higher Education Funding Council for England. The SDSS Web site is <http://www.sdss.org>. The SDSS is managed by the Astrophysical Research Consortium (ARC) for the Participating Institutions. The Participating Institutions are the American Museum of Natural History, the Astrophysical Institute Potsdam, the University of Basel, the University of Cambridge, Case Western Reserve University, the University of Chicago, Drexel University, Fermilab, the Institute for Advanced Study, the Japan Participation Group, The Johns Hopkins University, the Joint Institute for Nuclear Astrophysics, the Kavli Institute for Particle Astrophysics and Cosmology, the Korean Scientist Group, the Chinese Academy of Sciences (LAMOST), Los Alamos National Laboratory, the Max Planck Institute for Astronomy (MPIA), the Max Planck Institute for Astrophysics (MPA), New Mexico State University, Ohio State University, the University of Pittsburgh, the University of Portsmouth, Princeton University, the United States Naval Observatory, and the

University of Washington.

REFERENCES

- Abazajian, K. N. et al. 2009, *ApJS*, 182, 543
 Allende Prieto, C., Beers, T. C., Wilhelm, R., Newberg, H. J., Rockosi, C. M., Yanny, B., Lee, Y. S. 2006, *ApJ*, 636, 804
 Beers, T. C. et al. 2002, *AJ*, 124, 931
 Behr, B. 2003, *ApJS*, 149, 101
 Bond, N.A. et al. 2010, *ApJ*, 718, 1
 Brown, W.R. et al. 2008, *AJ*, 135, 564
 Carollo, D. et al. 2007, *Nature*, 450, 1020
 Carollo, D. et al. 2010, *ApJ*, 712, 692
 Carney, B.W. et al. 2003, *AJ*, 125, 293
 Carney, B.W. et al. 2008, *AJ*, 135, 196
 Chen, Y. Q., Nissen P. E., Zhao G., et al. 2000, *A&AS*, 141, 491,
 Chen, Y. Q., Zhao G., & Zhao J. K. 2009, *ApJ*, 702, 1336
 Chiba, M., & Beers, T. C. 2000, *AJ*, 119, 2843
 Francis, C., & Anderson, E. 2009, *NewA*, 14, 615
 Fuchs, B. et al. 2009, *AJ*, 137, 4149
 Fukugita, M., Ichikawa, T., Gunn, J. E., Doi, M., Shimasaku, K., & Schneider, D. P. 1996, *AJ*, 111, 1748
 Fuhrmann, K. 1998, *A&A*, 338, 161
 Gilmore, G., & Reid, N. 1983, *MNRAS*, 202, 1025
 Ivezić, Z. et al. 2008, *ApJ*, 684, 287
 Kaempfer T.A., de Boer K.S., & Altmann M. 2005, *A&A*, 432, 879
 Kinman, T.D., Morrison, H.L., & Brown, W.R. 2009, *AJ*, 137, 3198
 Klement, R. et al. 2009, *ApJ*, 698, 865
 Majewski, S.R. 1992, *ApJS*, 78, 87
 Majewski, S. R. 1994, in *Astronomy from wide-field imaging: proceedings of IAU Symp. 161*, ed. H. T. McGillivray, E. B. Thomson, B. M. Lasker, I. N. Reid, D. F. Malin, R. M. West & H. Lorenz (Dordrecht: Kluwer), 425
 Munn, J. A. et al. 2008, *AJ*, 136, 895
 Nissen, P. E., & Schuster, W. J. 2010, *A&A*, 511, L10
 Piotto, G. et al. 2002, *A&A*, 391, 945
 Preston, G.W. 2006, *AJ*, 132, 85
 Rose, J.A. 1985, *AJ*, 90, 787
 Schlegel, D. J., Finkbeiner, D. P., & Davis, M. 1998, *ApJ*, 500, 525
 Straizys V., Bartkevicius A., & Sperauskas J. 1981, *A&A*, 99, 152
 Soubiran, C., Bienaymé, O., & Siebert, A. 2003, *A&A*, 398, 141
 Tautvaisiene, G. 1996, *Baltic Astronomy*, 1996, 5, 503
 Turon, C., et al. 2005, 39TH ESLAB Symposium on Trends in Space Science and Cosmic Vision 2020, (eds.) F. Favata, J. Sanz-Forcada, A. Giménez, and B. Battrick. ESA SP-588. European Space Agency, p.53
 Yanny, B., et al. 2009, *ApJ*, 700, 1282
 York, D. et al. 2000, *ApJ*, 120, 1579
 Zhao, G. et al. 2006, *ChJAA*, 6, 265